AGU PUBLICATIONS

JGR

Journal of Geophysical Research: Space Physics

RESEARCH ARTICLE
10.1002/2016JA023488

Special Section:
Major Results From the MAVEN Mission to Mars

MAVEN observations of tail current sheet flapping at Mars

Gina A. DiBraccio[1], Julian Dann[2], Jared R. Espley[1], Jacob R. Gruesbeck[1,3], Yasir Soobiah[1,3], John E. P. Connerney[1,4], Jasper S. Halekas[5], Yuki Harada[6], Charles F. Bowers[7], David A. Brain[7], Suranga Ruhunusiri[5], Takuya Hara[6], and Bruce M. Jakosky[7]

[1]Solar System Exploration Division, NASA Goddard Space Flight Center, Greenbelt, Maryland, USA, [2]Astronomy and Physics Departments, Wesleyan University, Middletown, Connecticut, USA, [3]Department of Astronomy, University of Maryland, College Park, Maryland, USA, [4]Space Research Corporation, Annapolis, Maryland, USA, [5]Department of Physics and Astronomy, University of Iowa, Iowa City, Iowa, USA, [6]Space Sciences Laboratory, University of California, Berkeley, California, USA, [7]Laboratory for Atmospheric and Space Physics, University of Colorado Boulder, Boulder, Colorado, USA

Key Points:
- MAVEN data analysis of tail current sheet dynamics at Mars reveals that steady global flapping occurs more often than kink-like local flapping
- A majority of the kink-like flapping events are generated by waves propagating in the opposite direction from the solar wind electric field
- Mars' tail exhibits similar flapping to Earth and Venus with different wave propagation directions suggesting different energy sources

Correspondence to:
G. A. DiBraccio,
gina.a.dibraccio@nasa.gov

Citation:
DiBraccio, G. A., et al. (2017), MAVEN observations of tail current sheet flapping at Mars, *J. Geophys. Res. Space Physics*, *122*, 4308–4324, doi:10.1002/2016JA023488.

Received 21 SEP 2016
Accepted 20 MAR 2017
Accepted article online 23 MAR 2017
Published online 19 APR 2017

©2017. American Geophysical Union. All Rights Reserved.

Abstract The Martian magnetotail is a complex regime through which atmospheric particles are lost to space. Our current understanding of Mars' tail continues to develop with the comprehensive particle and field data collected by Mars Atmosphere and Volatile EvolutioN (MAVEN). In this work, we identify periods when MAVEN encounters multiple current sheet crossings through a single tail traversal in order to understand tail dynamics. We apply an analysis technique that has been developed and validated by using multipoint measurements in order to separate the spatial and temporal properties associated with current sheet flapping. Events are classified into periods of steady flapping, due to a global motion of the current sheet, and kink-like flapping, resulting from localized wave propagation along the tail current sheet. Out of 106 periods during which multiple current sheet crossings were observed, 20 were due to steady flapping and 10 from kink-like flapping. A majority of the kink-like events resulted from waves propagating in the opposite direction of the solar wind convection electric field, regardless of their location in the tail, unlike at Earth and Venus. This finding suggests that possible magnetosphere energy sources, whereby plasma is accelerated and removed from the Martian environment, are not located in the central magnetotail; rather, these waves may be driven by a source located at the tail flank based on the direction of the solar wind electric field. Therefore, by identifying potential sources of impulsive energy release in the tail, we may better understand mechanisms that drive atmospheric loss at Mars.

1. Introduction

The Martian magnetosphere is formed as a result of direct solar wind interaction with the planetary atmosphere. This interaction is complicated by the existence of crustal magnetic fields covering a majority of the planet with the most intense sources located in the southern hemisphere, centered near 180° longitude [*Acuña et al*., 1998; *Connerney et al*., 2005]. The induced magnetotail forms as the Sun's interplanetary magnetic field (IMF), carried by the solar wind, drapes around Mars (see review by *Crider et al*. [2004]). The nature of the Martian magnetotail has been highly debated: early observations from Mars 2, 3, and 5, along with Phobos 2, indicated that the tail was purely induced in a comet- or Venus-like formation [*Yeroshenko et al*., 1990; *Dubinin et al*., 1991; *Vaisberg*, 1992]. *Luhmann et al*. [1991] found that the Martian tail is less severely draped than that of Venus, with an average flaring angle of 23° at a distance of 2.7 R_M downtail (where R_M is the radius of Mars, or 3397 km) and a more extensive study by *Zhang et al*. [1994] demonstrated that this tail flaring is strongly controlled by upstream solar wind pressure, similar to the dynamics at Earth. A review by *Lundin and Barabash* [2004] addressed several other similarities between the magnetotails of Earth and Mars, including a high-density plasma sheet and an enhanced field strength associated with the lobes. In an analysis of Mars Global Surveyor data, *Romanelli et al*. [2015] showed that the orientation and spatial extent of the Martian magnetotail lobes are highly dependent on the IMF direction.

More recently, Mars Atmosphere and Volatile EvolutioN (MAVEN) [*Jakosky et al*., 2015] observations have suggested that the magnetotail is much more complex, demonstrating the need to further explore this region of the Martian magnetosphere. *Luhmann et al*. [2015] analyzed MAVEN magnetic field and electron data to assess the complex field topology in the tail, suggesting that the Martian magnetotail configuration appears to be a hybrid between induced and intrinsic magnetospheres. MAVEN has also made great progress in terms

of the tail plasma dynamics: tailward escape of planetary ions has been observed in the form of plasma clouds [*Halekas et al*., 2016], detached magnetic flux ropes [*DiBraccio et al*., 2015; *Hara et al*., 2015, 2016], bulk acceleration due to magnetic reconnection [*Harada et al*., 2015a], and the tailward transport of suprathermal (>25 eV) planetary ions [*Brain et al*., 2015; *Dong et al*., 2015; *Harada et al*., 2015b].

While a majority of the MAVEN magnetotail work has focused on plasma dynamics and atmospheric escape, this picture cannot be complete without a firm understanding of tail magnetic field dynamics. More specifically, we do not fully understand whether plasma energization occurs in the magnetotail current sheet and, if so, how this contributes to its removal from the system. This issue is exactly what we aim to investigate here: the role of the tail current sheet in atmospheric escape Mars.

An induced magnetotail resulting from the upstream IMF draped around the planet consists of two magnetic lobes, defined by uniform magnetic fields oriented in opposite directions that are separated by a central current sheet. This cross-tail current sheet, and the surrounding plasma sheet, has been identified as a main escape channel at Mars [*Dubinin et al*., 1993, 2011; *Fedorov et al*., 2006; *Barabash et al*., 2007]. The Martian crustal fields add a layer of complexity to the magnetotail structure by introducing low-altitude current sheets [*Halekas et al*., 2006], creating an environment that is fundamentally different from the induced and intrinsic magnetospheres of Venus and Earth, respectively. Exploring current sheets in the magnetotail of Mars is important for understanding particle acceleration and atmospheric loss processes because current sheets provide information on kinetics and global dynamics. For example, observations of current sheet thickness and local plasma characteristics can elucidate whether ion or electron scales drive the system. Additionally, particle acceleration resulting from tailward $\mathbf{J}\times\mathbf{B}$ forces and magnetic reconnection has been observed in the tail current sheet [*Dubinin et al*., 2011, 2012; *Eastwood et al*., 2008; *Halekas et al*., 2009; *DiBraccio et al*., 2015; *Harada et al*., 2015a].

At Mars, the tail current sheet's configuration is responsive to the orientation of the IMF and can change dramatically for various clock angles. It is not uncommon to observe multiple current sheet crossings on any given orbit as MAVEN passes through the Martian magnetotail. These multiple crossings may be due to a variety of factors: (1) the rotation of the tail in response to a change in the upstream IMF, (2) the existence of multiple current sheets due to open crustal fields that have been reconnected and stretched out in the tail [*Luhmann et al*., 2015], (3) a steady flapping of the current sheet in response to environmental changes such as upstream solar wind pressure, and (4) a kink-like flapping due to waves propagating along the current sheet, creating local perturbations through which the spacecraft may cross multiple times. We will explore the latter two mechanisms in this study, using an analysis technique previously applied to the magnetotails of Earth [*Rong et al*., 2015a] and Venus [*Rong et al*., 2015b] (discussed in section 3). For this approach, we simplify our view of the complex Martian magnetotail and assume that the draped IMF creates the tail current sheet, without much influence from open crustal magnetic fields.

Here we investigate steady and kink-like flapping of the cross-tail current sheet of the Martian magnetosphere by implementing the methods developed by *Rong et al*. [2015a, 2015b]. Utilizing the full suite of plasma and magnetic field observations from the MAVEN spacecraft, we assess the dynamics of the Martian tail current sheet and compare these results to Earth and Venus. We observe both steady and kink-like flapping in the magnetotail; however, unlike at Earth and Venus, a majority of the kink-like events are caused by waves propagating in the opposite direction of the solar wind convection electric field.

2. MAVEN Data

The MAVEN spacecraft was inserted into orbit about Mars on 21 September 2014 and, after a brief commissioning phase, began its primary science investigation on 16 November 2014. MAVEN's 4.5 h elliptical orbit reaches periapsis and apoapsis altitudes of ~150 km and ~6200 km, respectively. The 74° inclination orbit provides global coverage of the Martian space environment, sampling a full range of latitudes and local times over the course of its orbital evolution.

MAVEN's Magnetometer (MAG) [*Connerney et al*., 2015] provides vector magnetic field measurements at a maximum sampling rate of 32 vectors s^{-1}. These data are of primary importance in current sheet identification in the Martian magnetotail. We utilize the MAG data in two coordinates systems: The first is Mars Solar Orbital (MSO) coordinates, where X_{MSO} is directed from the center of the planet toward the center of the

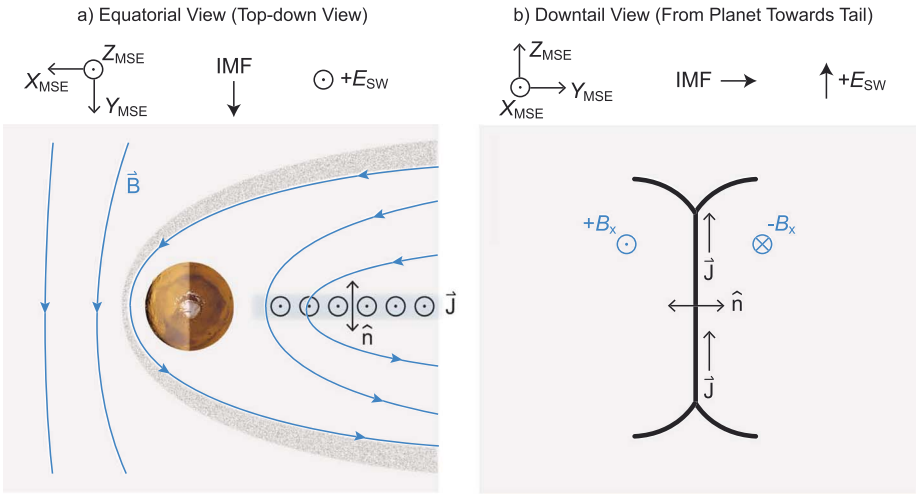


Figure 1. Schematic views of the Martian magnetosphere in Mars Solar Electric (MSE) coordinates. (a) An equatorial view in the X_{MSE}-Y_{MSE} plane where the IMF is oriented in the $+Y_{MSE}$ direction, creating a dual-lobe tail as demonstrated by the magnetic field lines (blue lines with arrows). The resulting cross-tail current sheet (encircled dot) and the solar wind convection electric field ($\mathbf{E_{SW}}$) are oriented in the Z_{MSE} direction with the current sheet normal ($\hat{\mathbf{n}}$) in the Y_{MSE} direction. In this schematic, the orientation of the planet (i.e., view of the northern hemisphere) refers to the case where the IMF is oriented in the $+Y_{MSE}$ direction prior to the coordinate system transformation. (b) A downtail view, from Mars toward the magnetotail, of the dual-lobe induced tail configuration in MSE coordinates. The lobe magnetic fields are oriented in the $+X_{MSE}$ (encircled dot) and $-X_{MSE}$ (encircled cross) directions and are separated by the cross-tail current sheet (thick black line), **J**, oriented in the $+Z_{MSE}$ direction.

Sun, Y_{MSO} points opposite to the direction of Mars' orbital velocity component, and Z_{MSO} completes the right-handed system. In the MSO coordinate system, magnetotail current sheet crossings are identified by a change of polarity in the $B_{X,MSO}$ component. This signature is observed in $B_{X,MSO}$ regardless of IMF orientation because the fields are oriented predominantly in the $\pm X_{MSO}$ direction in the tail.

The second coordinate system utilized here is the Mars Solar Electric (MSE) coordinate system. This involves a transformation in the *Y-Z* plane by calculating the direction of the solar wind convection electric field ($\mathbf{E_{SW}}$) on the basis of the antisunward solar wind flow ($\mathbf{V_{SW}}$) in the $-X_{MSO}$ direction and IMF orientation ($\mathbf{B_{IMF_YZ}}$) perpendicular to the solar wind flow: $\mathbf{E_{SW}} = -\mathbf{V_{SW}} \times \mathbf{B_{IMF_YZ}}$. Vectors are transformed such that $\mathbf{E_{SW}}$ is positive along the Z_{MSE} direction, and therefore, $\mathbf{B_{IMF_YZ}}$ and $-\mathbf{V_{SW}}$ are oriented in the directions of Y_{MSE} and X_{MSE}, respectively. This MSE system organizes the draped IMF into two tail lobes, separated by a cross-tail current sheet oriented in the X_{MSE}-Z_{MSE} plane at midnight local time (a 90° rotation from the intrinsic magnetotail of Earth with north-south lobes) where the current sheet normal is in the Y_{MSE} direction. A schematic of the MSE coordinate system is shown in Figure 1 for both an equatorial and a downtail view.

Data from MAVEN's Solar Wind Ion Analyzer (SWIA) [*Halekas et al.*, 2015] are analyzed to complement the magnetic field observations. SWIA measures the flux, energy, and distribution of ions throughout the Martian space environment at cadences up to ~4 s. These ion measurements are used to assist in the identification of times when MAVEN exits the magnetotail and enters the shocked solar wind in the magnetosheath.

3. Analysis Technique

We present an analysis of magnetotail current sheet flapping based on the technique first developed, validated, and implemented at Earth by *Rong et al.* [2015a] and then later successfully applied to Venus [*Rong et al.*, 2015b]. This technique (herein the "Rong method") augments our ability to deduce spatial and temporal variations during instances with multiple tail current sheet crossings, based on single-point measurements and minimum variance analysis (MVA) [*Sonnerup and Cahill*, 1967; *Sonnerup and Scheible*, 1998].

Rong et al. [2015a] utilized multipoint measurements from the Cluster mission [*Escoubet et al.*, 2001] to separate tail current sheet motion into two types of flapping (steady flapping and kink-like flapping),

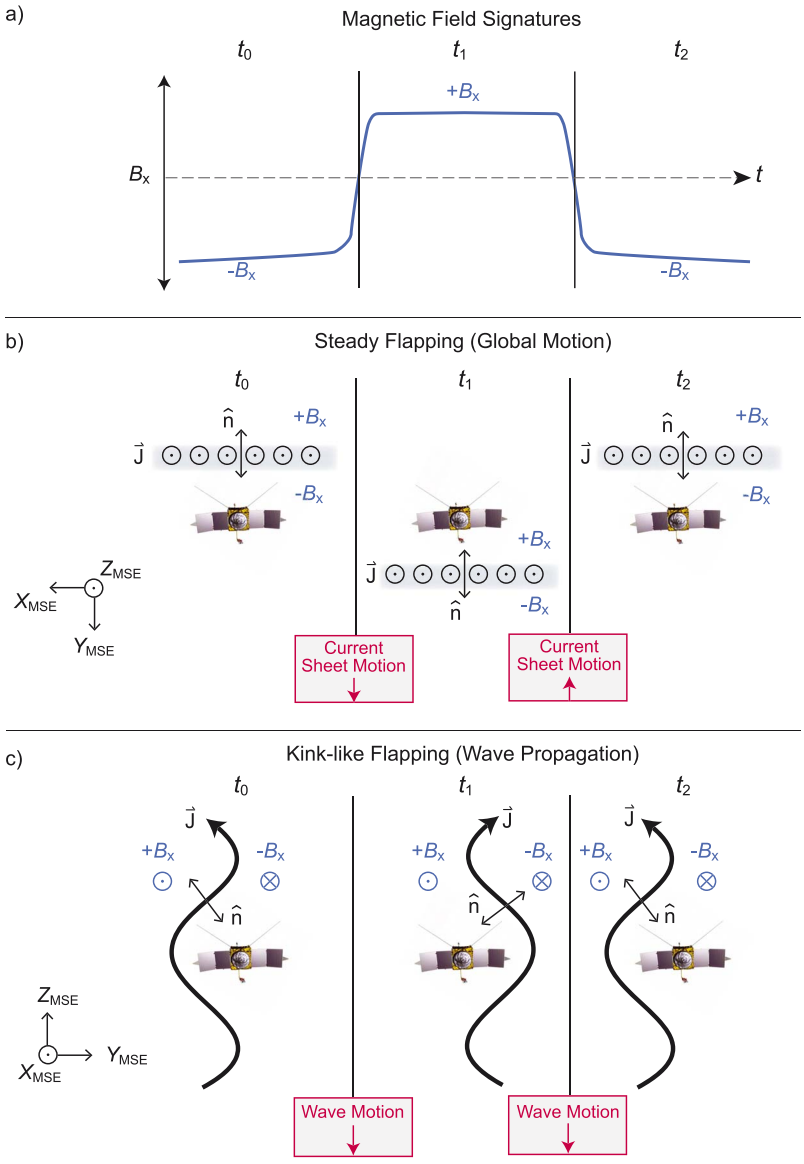


Figure 2. Schematics of dynamics resulting in multiple current sheet crossings of the Martian magnetotail. (a) Magnetic field signatures of multiple current sheet crossings are demonstrated by rotations in the B_X component (in both MSO and MSE coordinates) over three time intervals (t_0, t_1, and t_2). The magnetic field is oriented in the $-X_{MSO}$ direction during t_0, followed by a current sheet crossing (black vertical line), where the magnetic field becomes oriented in the $+X_{MSO}$ direction during t_1. A second current sheet crossing occurs as the field rotates back to a $-X_{MSO}$ orientation during t_2. Current sheet normal ($\hat{\mathbf{n}}$) is indicated by double-headed arrows. Magnetic fields are blue, and the current sheet ($\mathbf{J}$) is black. (b) An equatorial view (as explained in Figure 1a) of steady current sheet flapping, producing magnetic field rotations in the B_X component over time intervals t_0, t_1, and t_2. During t_0, the spacecraft is in the $-B_X$ lobe until the current sheet (encircled dot) moves in the $+Y_{MSE}$ direction such that the spacecraft is in the $+B_X$ lobe during interval t_1. As the global flapping motion continues, the current sheet moves in the $-Y_{MSE}$ direction and the spacecraft is once again in the $-B_X$ lobe. (c) A downtail view (see Figure 1b) of kink-like flapping of the current sheet (thick black line) created by waves propagating in the Y_{MSE}-Z_{MSE} plane. For this example, the wave is propagating in the $-Z_{MSE}$ direction. The spacecraft is in the $-B_X$ lobe during t_0 and enters the $+B_X$ lobe in t_1 due to wave motion along the current sheet. As this motion continues, the spacecraft enters back into the $-B_X$ lobe in t_2. The magnetic field signatures in B_X (Figure 2a) may be a result of either steady flapping (Figure 2b) or kink-like flapping (Figure 2c).

illustrated in Figure 2. Steady flapping involves a global motion of the current sheet as it moves back and forth over the spacecraft, causing multiple current sheet crossings. For this type of flapping, the spacecraft will cross the same region of the current sheet and the normal direction ($\hat{\mathbf{n}}$) remains relatively steady. This flapping motion does not propagate along the current sheet as a wave. Conversely, the kink-like flapping motion results from waves propagating along the tail current sheet, causing the normal direction to alternate in the Y_{MSE}-Z_{MSE} plane, as indicated in Figure 2c. These waves typically travel along the Z_{MSE} direction, either in the $+\mathbf{E_{SW}}$ or $-\mathbf{E_{SW}}$ direction. Propagations in the X_{MSE}-Z_{MSE} plane may also be examined; however, our results in section 4 indicate that the n_x component of $\hat{\mathbf{n}}$ is negligible.

It is important to appreciate that the magnetic field time series of a current sheet crossing due to either steady or kink-like flapping will produce the same signature based on single-point measurements: MAG data will reveal a change in polarity in the B_X component as the field rotates (see Figure 2a). The spatial and temporal changes cannot be captured from these data alone. For this reason, the Rong method has provided an opportunity to dive deeper into these multiple current sheeting crossing signatures in order to understand variations in planetary magnetotails utilizing available observations.

Using single-point and multipoint Cluster observations of both steady and kink-like flapping, *Rong et al*. [2015a] developed and validated a robust technique to diagnose these flapping dynamics from single-point measurements. The technique separates periods of multiple current sheet crossings into steady and kink-like flapping, while determining the direction of wave propagation for the latter category. This method is useful at Earth; however, it is even more beneficial at other planets where spatial and temporal analyses are hindered by the limitations of single-point observations. The Rong method was successfully utilized at Venus [*Rong et al*., 2015b] to understand the dynamics of this induced magnetotail, and now we apply it to Mars.

We begin by identifying periods when MAVEN observed multiple current sheet crossings within the magnetotail. MAG data are examined in MSO coordinates, and the current sheet crossings are identified as polarity changes in B_X as the magnetic field rotates from one lobe to the next. We require a minimum of three current sheet crossings within a given orbit in order to select an event for further investigation. It is important to select complete current sheet crossings, rather than intervals where the current sheet only partially passes over the spacecraft before returning to its previous orientation. A complete current sheet crossing is characterized by a sudden decrease in B as all three magnetic field components approach zero. Additionally, B_X must exhibit a full 180° rotation during which the magnitude of B_X becomes approximately equal to that of the background tail lobe. During a partial current sheet crossing these conditions are not met because the entire field rotation is not observed. Therefore, the field magnitude does not decrease or the magnitude of B_X does not reach values similar to the background fields as the polarity changes.

Once a multiple current sheet-crossing event has been identified, MAG vectors are transformed into MSE coordinates based on solar wind measurements obtained upstream of the bow shock (see section 3.1 in *Halekas et al*. [2017] for information on these upstream data). The algorithm developed by *Halekas et al*. [2017] applies strict criteria on MAG measurements and SWIA onboard moments in order to ensure that only periods characterized by undisturbed, steady solar wind conditions are selected. In particular, the algorithm selects periods of stable IMF by setting a criterion for the normalized magnetic field fluctuation levels (σ_B/B), where σ_B is the root-sum-squared value of all three magnetic field components calculated over 4 s intervals. In order to be selected, upstream solar wind intervals must have $\sigma_B/B < 0.15$ along with other bulk plasma parameter criteria described by *Halekas et al*. [2017]. These data were processed over the entire mission in order to select all periods when MAVEN's orbit undoubtedly measured the upstream solar wind.

The thresholds set by *Halekas et al*. [2017] implement a conservative approach to identifying intervals when MAVEN observed upstream IMF conditions. Therefore, periods where IMF orientations produce upstream magnetic fluctuations, such as intervals with radial IMF, may not be included in the data set. As a final check for stable IMF, we examined the upstream orientation over consecutive orbits (when available) to remove any events for which the IMF may have exhibited large rotations while MAVEN traversed the tail. Once we have ensured that the IMF was stable, we utilize these upstream intervals to transform the MAG data from MSO into MSE coordinates. The MSE system allows us to define the nominal normal direction of the current sheet in the Y_{MSE} direction, based on the IMF draping pattern.

Next, MVA is applied to the MAG data over every individual current sheet encounter to determine the current sheet normal direction ($\hat{\mathbf{n}}$) by transforming the data into boundary-normal coordinates. Specifically, $\hat{\mathbf{n}}$ is determined by the minimization of a magnetic field covariance matrix, which calculates the eigenvalues and associated eigenvectors (see *Sonnerup and Scheible* [1998]). The resulting eigenvectors form an orthogonal system and represent the directions of minimum (B_1), intermediate (B_2), and maximum variance (B_3) in the magnetic field. In this MVA coordinate system, B_1 is equivalent to the normal direction because the normal component of the magnetic field is conserved across a discontinuity (i.e., the current sheet). Components B_2 and B_3 complete the Cartesian system and are free to rotate within the plane of the current sheet in response to field variations. These calculated eigenvectors, however, may be parallel or antiparallel to the resulting direction such that direction such that a 180° rotation of the transformation matrix may be required. This implies that acceptable normal directions are $\pm\hat{\mathbf{n}}$.

The accuracy of the MVA results is inferred by the ratios of the corresponding eigenvalues (λ_1, λ_2, and λ_3). A high intermediate-to-minimum eigenvalue ratio (λ_2/λ_1) indicates that the normal vector is well determined for a given current sheet crossing. For this reason, we require $\lambda_2/\lambda_1 \geq 3$ in order to accept a particular current sheet event for further analysis. Because we are interested in $\hat{\mathbf{n}}$, it is not necessary to limit the maximum-to-intermediate eigenvalue ratio (λ_3/λ_2); however, these ratios are typically very large (as shown in the examples in sections 4.1 and 4.2).

The most crucial part of the Rong method is calculating the "*k*-value" for each identified crossing (equation (1)). The pattern of *k* throughout the orbit reveals the flapping type. This *k* parameter is dependent on the components of $\hat{\mathbf{n}}$ in the plane that the wave propagation occurs. For waves occurring in the Y_{MSE}-Z_{MSE} plane, n_y and n_z are assessed by taking the cross product of the two and determining whether the sign of this result is positive (+) or negative (−). The sign change of B_X during the crossing, denoted as ΔB_X, factors into the calculation of *k*. For cases of $-B_X$ to $+B_X$, the sign is positive (+) or $\Delta B_X > 0$ and in the opposite case where the field changes from $+B_X$ to $-B_X$, the sign is negative (−) or $\Delta B_X < 0$. Using these parameters, we calculate *k* in the Y_{MSE}-Z_{MSE} plane:

$$k = \text{sign}\left(n_y \times n_z\right) \times \text{sign}(\Delta B_X). \tag{1}$$

Applying equation (1) to each crossing in a multiple current sheet series results in a sequence of *k* values that establish the flapping type. An alternating pattern between +1 and −1 indicates that steady flapping was occurring. In contrast, a sequence in which *k* is always +1 or always −1 identifies kink-like flapping events. The direction of wave propagation for kink-like flapping events is determined by the sign of *k*: propagation along the $+\mathbf{E_{SW}}$ direction ($+Z_{MSE}$) for $k = +1$ and $-\mathbf{E_{SW}}$ direction ($-Z_{MSE}$) for $k = -1$. This technique does not establish the flapping motion for each and every multiple crossings event. In those cases where neither an alternating nor constant pattern of *k* appears, we categorize these events as inconclusive. Equation (1) may be altered to analyze propagations in the X_{MSE}-Z_{MSE} plane by substituting n_y for n_x:

$$k = \text{sign}(n_x \times n_z) \times \text{sign}(\Delta B_X). \tag{2}$$

The flowchart in Figure 3 depicts each step necessary to establish both the flapping type (i.e., steady or kink-like) and the direction of the propagation (for kink-like events). In addition to determining the wave-propagation direction for kink-like flapping events from the sign of the *k* values, Figures 3a–3d illustrate the four possible scenarios as well. In each of these cases, it is important to consider whether the magnetic field is first oriented in the $+X_{MSE}$ or $-X_{MSE}$ direction. From there, one must assess whether the n_y and n_z have the same sign or opposite signs. With this information it is possible to determine the direction of wave propagation causing the kink-like current sheet flapping.

4. Results

We manually examined all orbits when MAVEN measured both the upstream solar wind and the magnetotail while avoiding periods when the spacecraft did not enter either the solar wind or the magnetotail, as a result of MAVEN's orbital periapsis evolution. We utilized the crustal magnetic field spherical harmonic model of *Morschhauser et al.* [2014] to ensure that the crustal fields were not mistaken for current sheet crossings. The MVA intervals were selected to include the entire current sheet crossing with only a short period of background tail lobe field on either side of the discontinuity. Once a multiple current sheet-crossing event is

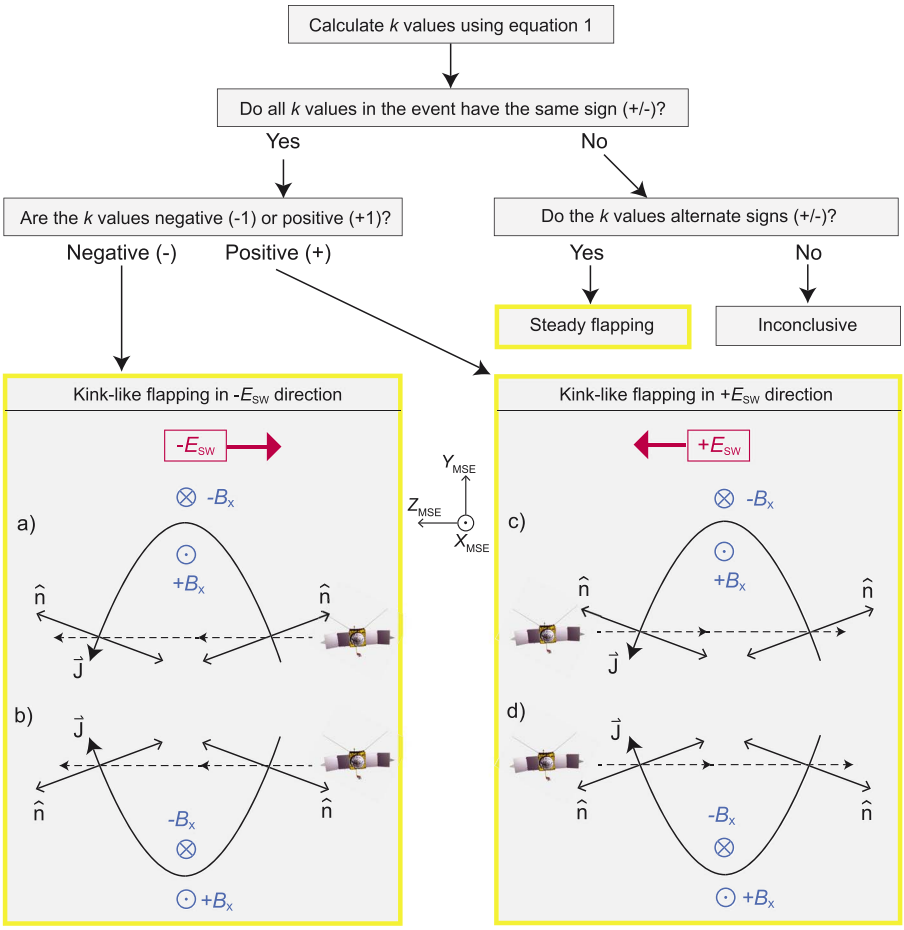


Figure 3. Flow chart for applying the Rong method to current sheet flapping. Schematics of four scenarios resulting in kink-like flapping are included. The current sheet (parabolic black line), current sheet normal $\hat{\mathbf{n}}$ (double-headed arrows), and the apparent spacecraft motion (dashed line) as the propagation moves along the current sheet are indicated. The blue encircled dot and encircled cross represent the $+B_X$ and $-B_X$ magnetic field lobes, respectively. The highlighted yellow boxes indicate the steady and kink-like solutions. Kink-like flapping with wave propagation in the $-\mathbf{E_{SW}}$ direction. (a) The spacecraft observes the magnetic field in the $-X_{MSO}$ direction until the current sheet crosses the spacecraft, where n_y and n_z have opposite signs, and then observes the magnetic field in the $+X_{MSO}$ direction. The current sheet crosses the spacecraft once again, where n_y and n_z have the same sign, and then observes the field in the $-X_{MSO}$ direction. (b) The spacecraft observes the magnetic field in the $+X_{MSO}$ direction until the current sheet crosses the spacecraft, where n_y and n_z have the same sign, and then observes the magnetic field in the $-X_{MSO}$ direction. The current sheet crosses the spacecraft once again, where n_y and n_z have opposite signs, and then observes the field in the $+X_{MSO}$ direction. Kink-like flapping with wave propagation in the $+\mathbf{E_{SW}}$ direction. (c) The spacecraft observes the magnetic field in the $-X_{MSO}$ direction until the current sheet crosses the spacecraft, where n_y and n_z have the same sign, and then observes the magnetic field in the $+X_{MSO}$ direction. The current sheet crosses the spacecraft once again, where n_y and n_z have opposite signs, and then observes the field in the $-X_{MSO}$ direction. (d) The spacecraft observes the magnetic field in the $+X_{MSO}$ direction until the current sheet crosses the spacecraft, where n_y and n_z have opposite signs, and then observes the magnetic field in the $-X_{MSO}$ direction. The current sheet crosses the spacecraft once again, where n_y and n_z have the same sign, and then observes the field in the $+X_{MSO}$ direction. Adapted from *Rong et al.* [2015b].

identified and accepted based on the MVA analysis criteria, we apply the Rong method to calculate the *k* value and diagnose the flapping type. We identified occurrences of both steady and kink-like flapping activity in the Martian magnetotail by using the following steps:

1. Examine MAVEN orbits where the spacecraft measures both the upstream solar wind and the magnetotail.
2. Identify orbits with a minimum of three current sheet crossings for further analysis, using the *Morschhauser et al.* [2014] model to avoid confusion with crustal fields.
3. Transform the MAG data from MSO into MSE coordinates.

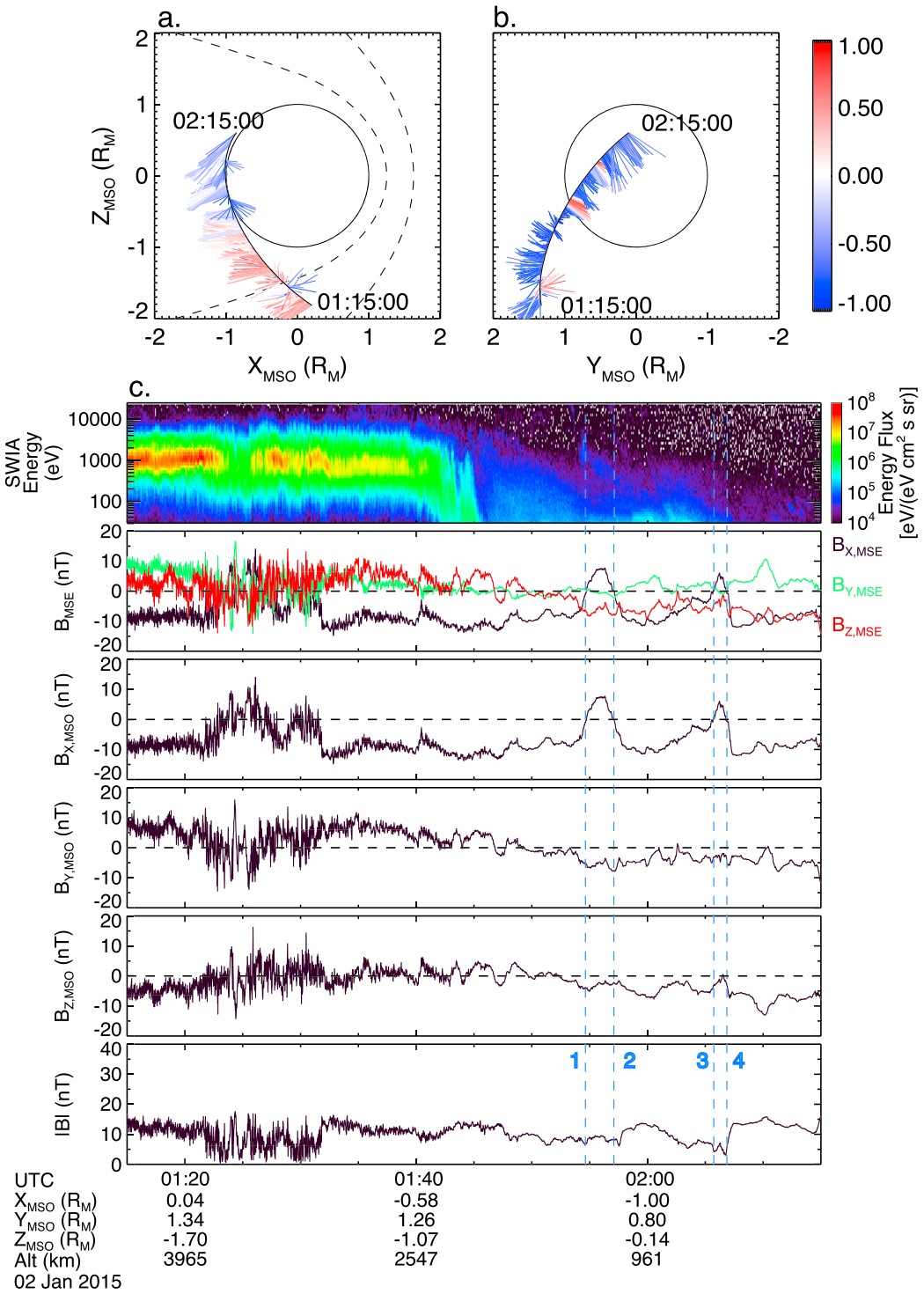


Figure 4. A portion of MAVEN's orbit on 2 January 2015 (corresponding to time series) viewed from (a) the meridional (X_{MSO}-Z_{MSO}) plane and (b) behind the planet toward the Sun (Y_{MSO}-Z_{MSO}) when steady current sheet flapping occurred. Nominal IMB and bow shock positions [*Trotignon et al.*, 2006] are indicated by dashed lines. Normalized magnetic field vector projections are plotted along the trajectory where the red-blue color scale represents the normalized out-of-plane component: B_Y (Figure 4a) and B_X (Figure 4b). (c) MAVEN plasma and magnetic field data from top to bottom: SWIA ion energy spectra, magnetic field in MSE coordinates, B_X in MSO coordinates, B_Y in MSO coordinates, B_Z in MSO coordinates, and total field magnitude $|B|$. The blue vertical dashed lines indicate selected current sheet crossings (labeled 1, 2, 3, and 4).

4. Perform MVA on each individual current sheet crossing and accept events with $\lambda_2/\lambda_1 \geq 3$.
5. Calculate k value and diagnose flapping type based on the Rong method classification criteria (see Figure 3).

We analyzed all MAVEN orbits from 16 November 2014, the start of the primary mission science phase, through 31 October 2015. During this interval, a total of 504 orbits met our selection criteria. Examples of both steady and kink-like tail flapping events are presented in the following sections, along with preliminary statistics of tail flapping in the Martian magnetotail.

4.1. Steady Flapping Example

MAVEN encountered a series of current sheet crossings during a tail traversal on 2 January 2015 (orbit 502) as the spacecraft entered the southern tail in the premidnight sector and continued toward periapsis. We determined that this series of four current sheet crossings met the Rong method criteria for steady flapping.

Figures 4a and 4b illustrate MAVEN's trajectory from 01:15 UTC to 02:15 UTC on 2 January 2015. Figure 4a provides a meridional plane projection, while Figure 4b is the view from the tail toward the planet. The whiskers along the trajectory indicate the normalized magnetic field vector projections in MSO coordinates. The color is used to represent the normalized out-of-plane component: B_Y in Figure 4a and B_X in Figure 4b. The red-blue color scale assists in identification of polarity reversals of the field, particularly in Figure 4b where the excursions from blue to red indicate a rotation in the B_X component of the field—the key signature for tail current sheet crossings.

A time series plot of SWIA and MAG measurements during this orbital interval is shown in Figure 4c. From the top to bottom, we include the SWIA omni-directional energy spectra; magnetic field data in MSE coordinates (B_{MSE}); separate panels for MSO components B_X, B_Y, and B_Z; and the total field magnitude. At the beginning of this interval (01:15 UTC), MAVEN was located in the turbulent magnetosheath at a radial distance of ~2.16 R_M from the planet. The magnetosheath is identified by the high-frequency fluctuations in all components of the magnetic field, along with ion measurements of shocked solar wind plasma with a broad energy distribution peaking at ~1 keV. MAVEN crossed the induced magnetopause boundary (IMB) and entered the magnetosphere shortly after 01:40 UTC. At this time the flux of ions and magnetosheath wave activity both dramatically decreased and the field became much more stable. Examination of the B_X component reveals a series of four current sheet crossings (vertical dashed blue lines in Figure 4c) as the measured field alternates between the $-X_{MSO}$ and $+X_{MSO}$ directions. These current sheet crossings are also identified in the B_X component of the MSE coordinate system (black line in the B_{MSE} panel).

We performed a MVA on the MSE magnetic field data for each individual crossing and determined the current sheet normal directions. As an example, the MVA results for the fourth and final current sheet crossing (labeled 4 in Figure 4c) beginning at 02:06:26 UTC are shown in Figure 5. The time series in Figure 5a shows the magnetic field during the current sheet crossing in MVA coordinates, where B_1 is the field in the normal direction. The main field rotation of the current sheet crossing is identified in the maximum variance component, B_3, as the field rotates from ~ −5 nT to ~ +13 nT. The hodograms in Figures 5b and 5c further illustrate the change in field configuration characterized by the ~180° rotation in the B_2-B_3 plane. For this event, λ_2/λ_1 is 35.6, which is well above the required value of three. The current sheet normal is predominantly oriented in the Y_{MSE} direction with $\hat{\mathbf{n}} = \pm[0.21, 0.95, -0.24]$, as expected based on an induced IMF draping pattern in MSE coordinates.

Following the MVA characterization of each current sheet, we define ΔB_X for each crossing in order to calculate k. If the field transitions from $-B_X$ to $+B_X$ ($+B_X$ to $-B_X$) we define ΔB_X as +1 (−1). Using the value of ΔB_X, along with the normal vector from MVA, we calculate k by using equation (1).

The results for MVA, ΔB_X, and k over each of the four current sheet crossings on 2 January 2015 are listed in Table 1, along with the time and spacecraft location. The direction of $\hat{\mathbf{n}}$ deviates only slightly from Y_{MSE} and the k value alternates between +1 and −1, indicating steady flapping as the tail current sheet moves in a uniform motion.

4.2. Kink-Like Flapping Example

MAVEN observed kink-like flapping of the tail current sheet as the spacecraft passed near the midnight plane of Mars on 8 September 2015 (orbit 1834). The spacecraft trajectory during this event is illustrated in

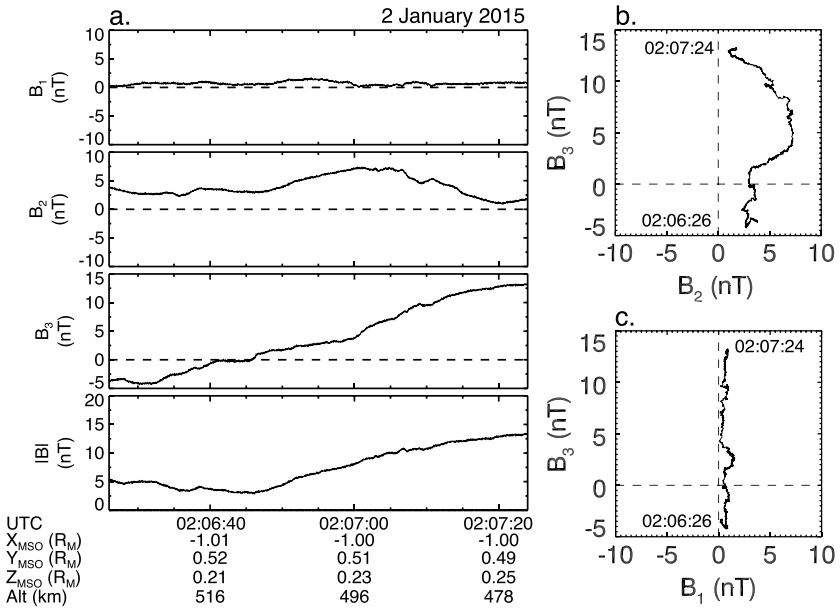


Figure 5. (a) MAG data during current sheet crossing #4 (see Figure 4) on 2 January 2015 in MVA coordinates. Magnetic field hodograms in the (b) B_2-B_3 and (c) B_1-B_3 planes.

Figures 6a and 6b, with views of the meridional plane (X_{MSO}-Z_{MSO}) and from the tail looking toward the planet (Y_{MSO}-Z_{MSO}), respectively. MAVEN was coming out of periapsis in the southern hemisphere as it traversed through the magnetotail and experienced three current sheet crossings before exiting in the northern magnetosheath. Once again, the whisker plots along the trajectory depict the normalized magnetic field projected into the plane where Figure 6a shows the B_Y component and Figure 6b demonstrates the polarity of B_X.

MAG and SWIA data collected during this interval are plotted in Figure 6c, with the same panels as described earlier in Figure 4c. Beginning at 07:00 UTC, following periapsis, MAVEN observed a relatively stable ~8 nT magnetic field predominantly oriented in the $+X_{MSO}$ direction and low plasma fluxes, as expected in the tail. The vertical dashed blue lines mark the three current sheet traversals, identified as a change in polarity of B_X, in both MSO and MSE, and a decrease in $|B|$. Crossings 1 and 2 occur within several minutes of each other before the field rotated to $+B_X$ for an ~20 min interval. At ~07:30 UTC, MAVEN observed a partial current sheet crossing as the field briefly rotated to $B_X \sim 0$ nT without a full transition into the $-B_X$ tail lobe while B remained relatively stable; therefore, this crossing is not included in our analysis. The third and final crossing occurred minutes later as the field rotated to a $-B_X$ orientation with a field strength of ~9 nT. The field remained in this direction as MAVEN exited the magnetosphere and began observing the high-frequency magnetosheath wave activity along with a sudden increase in ion flux.

Using the MAG data in MSE coordinates (Figure 6c), we performed a MVA on all three current sheet crossings. The MVA results for the second current sheet encounter occurring at 07:13:18 UTC (labeled 2 in Figure 6c) are shown in Figure 7. The time series of the magnetic field transformed into minimum variance coordinates (Figure 7a) shows the main current sheet rotation in B_3, or the maximum variance component, as the field

Table 1. Analysis Results for Current Sheet Crossings During Orbit 502 on 2 January 2015

	UTC (hh:mm:ss)	Location [X_{MSO}, Y_{MSO}, Z_{MSO}]	λ_3/λ_2	λ_2/λ_1	$\hat{\mathbf{n}}$	Sign (ΔB_X)	k
1	01:54:52	[−0.91, 0.99, −0.45]	23.1	25.9	[0.10, 0.94, −0.31]	+1	−1
2	01:56:02	[−0.95, 0.93, −0.34]	17.3	11.3	[0.03, 0.63, −0.78]	−1	+1
3	02:05:07	[−1.01, 0.59, 0.13]	27.7	6.40	[0.40, 0.63, −0.67]	+1	−1
4	02:06:26	[−1.01, 0.53, 0.20]	10.4	33.5	[0.21, 0.95, −0.24]	−1	+1

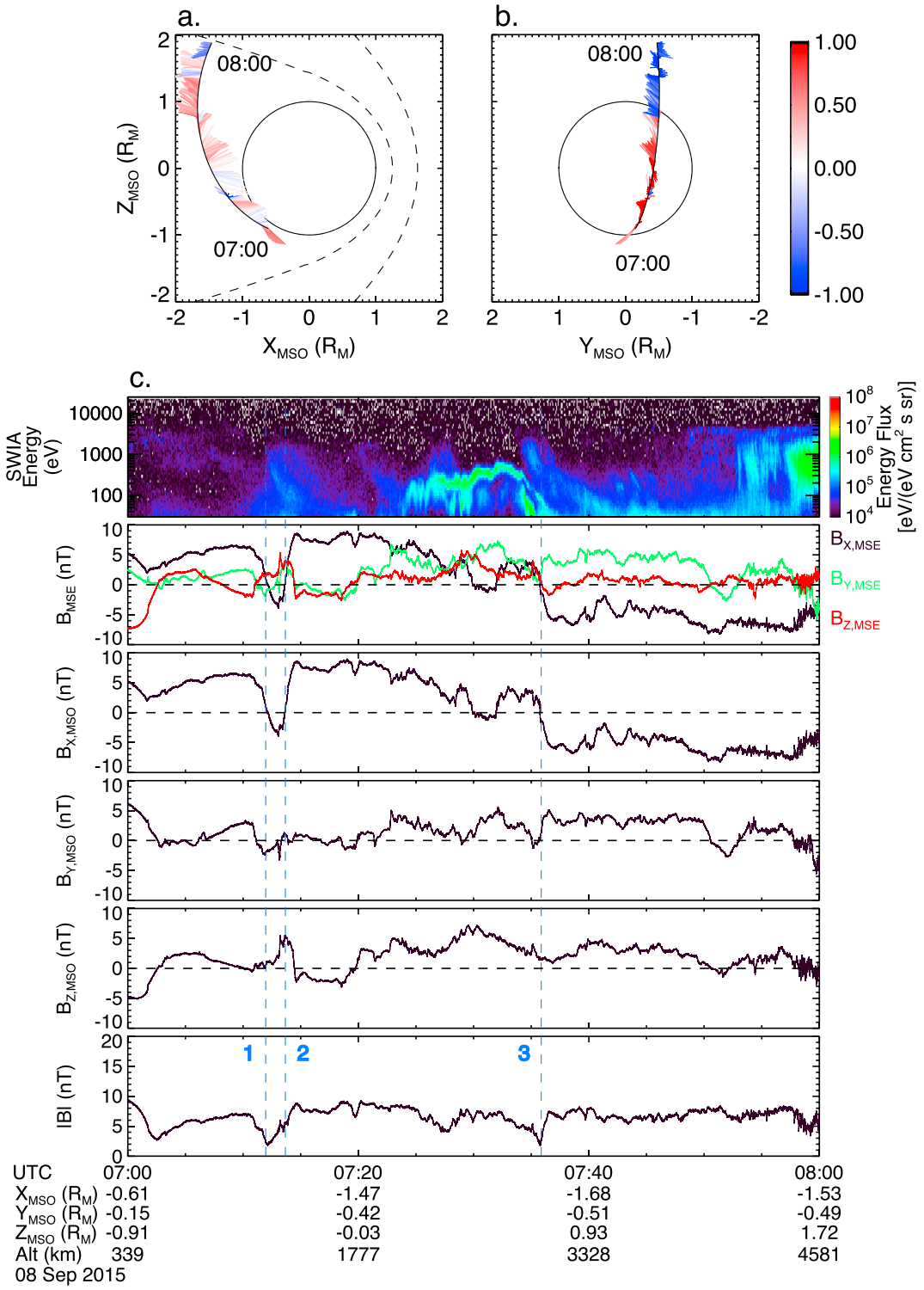


Figure 6. A portion of MAVEN's orbit on 8 September 2015 (corresponding to time series) viewed from (a) the meridional (X_{MSO}-Z_{MSO}) plane and (b) behind the planet toward the Sun (Y_{MSO}-Z_{MSO}) when kink-like current sheet flapping occurred. Nominal IMB and bow shock positions [*Trotignon et al.*, 2006] are indicated by dashed lines. Normalized magnetic field vector projections are plotted along the trajectory where the red-blue color scale represents the normalized out-of-plane component: B_Y (Figure 6a) and B_X (Figure 6b). (c) MAVEN plasma and magnetic field data from top to bottom: SWIA ion energy spectra, magnetic field in MSE coordinates, B_X in MSO coordinates, B_Y in MSO coordinates, B_Z in MSO coordinates, and total field magnitude $|B|$. The blue vertical dashed lines indicate selected current sheet crossings (labeled 1, 2, and 3).

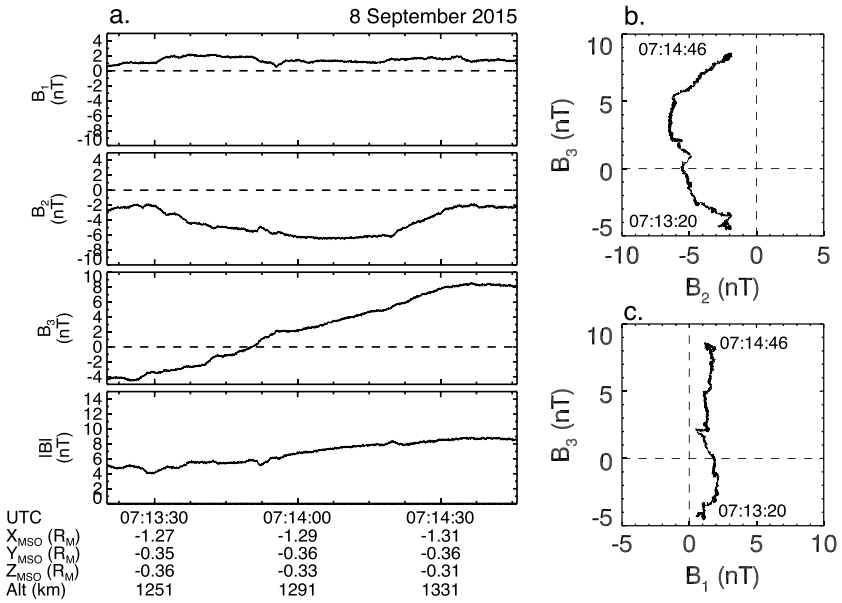


Figure 7. (a) MAG data during current sheet crossing #2 (see Figure 6) on 8 September 2015 in MVA coordinates. Magnetic field hodograms in the (b) B_2-B_3 and (c) B_1-B_3 planes.

varied from −4 nT to +8 nT. In the minimum variance direction (B_1), the field remains relatively constant and near 0 nT as MAVEN crossed through the current sheet. Magnetic field hodograms are presented in Figures 7b and 7c where the large ~180° rotation of the field is illustrated B_2-B_3 plane. The eigenvalue ratios are above the minimum criterion of three with $\lambda_2/\lambda_1 = 19.2$. As expected of the draped IMF in MSE coordinates, the normal current sheet direction was oriented principally in the Y_{MSE} direction where $\hat{\mathbf{n}} = \pm[0.10, 0.91, -0.40]$.

We calculate k (equation (1)) after applying MVA to all three current sheet crossings by defining ΔB_X and utilizing our knowledge of $\hat{\mathbf{n}}$. The results of this current sheet analysis on 8 September 2015 are listed in Table 2. The normal directions alternate between the Y_{MSE} and Z_{MSE} directions for successive crossings, suggesting possible wave propagation, or kink-like flapping. The k values remain constant at −1 for all three crossings, confirming that MAVEN observed kink-like flapping at this time; the current sheet is locally distorted by wave propagation along the Y_{MSE}-Z_{MSE} plane (supported by the variation in $\hat{\mathbf{n}}$). The Rong method was designed such that the sign of k indicates the direction of wave propagation to give clues on energy sources throughout the magnetotail. For this example, k is negative, meaning that the waves are traveling in the $-Z_{MSE}$ direction or opposite to the convection electric field of the solar wind, $\mathbf{E_{SW}}$. This example corresponds to the scenario illustrated in Figure 2c. The magnetic field begins in the $+B_X$ direction, rotates to $-B_X$, and then back to $+B_X$ again. During the first and third crossings, n_y and n_z have the same sign; however, during the second crossing, n_y and n_z have opposite signs. This observation strengthens the conclusion that this multiple current sheet crossing event was created by waves propagating along the current sheet in the $-\mathbf{E_{SW}}$ direction.

4.3. Statistics

The examples presented in sections 4.1 and 4.2 show that both steady and kink-like flapping of the tail current sheet occurs at Mars. We now present preliminary statistics on these magnetotail flapping dynamics in order to determine which of the two flapping types is more prevalent.

Table 2. Analysis Results for Current Sheet Crossings During Orbit 1834 on 8 September 2015

	UTC (hh:mm:ss)	Location (R_M) [X_{MSO}, Y_{MSO}, Z_{MSO}]	λ_3/λ_2	λ_2/λ_1	$\hat{\mathbf{n}}$	Sign (ΔB_X)	k
1	07:10:28	[−1.16, −0.32, −0.50]	8.28	19.8	[0.07, 0.67, 0.74]	−1	−1
2	07:13:18	[−1.27, −0.35, −0.37]	7.38	19.2	[0.10, 0.91, −0.40]	+1	−1
3	07:35:26	[−1.67, −0.50, 0.72]	31.4	16.5	[−0.18, 0.42, 0.89]	−1	−1

Table 3. MAVEN Statistical Results of Mars Current Sheet Flapping Events

	Date (dd-mm-yyyy)	UTC (hh:mm:ss)	Location (R_M) [X_{MSO}, Y_{MSO}, Z_{MSO}]	N	λ_2/λ_1	Flapping Type	$\pm\boldsymbol{E_{SW}}$
1	01-12-2014	00:00:46	[−1.44, −0.12, −0.12]	3	3.0	Kink	$-E_{SW}$
2	03-12-2014	16:05:58	[−1.55, 0.22, −0.64]	3	8.9	Steady	
3	06-12-2014	03:39:38	[−1.50, 0.47, −0.94]	3	6.6	Steady	
4	08-12-2014	15:28:56	[−1.44, 0.23, −0.31]	5	4.6	Steady	
5	10-12-2014	13:11:32	[−1.43, 0.49, −0.67]	5	4.9	Steady	
6	11-12-2014	03:06:40	[−1.38, 0.23, −0.17]	3	8.0	Steady	
7	11-12-2014	07:25:44	[−1.38, 0.65, −0.93]	4	3.0	Kink	$-E_{SW}$
8	13-12-2014	00:47:58	[−1.39, 0.53, −0.59]	5	3.2	Steady	
9	13-12-2014	09:42:58	[−1.21, 0.88, −1.23]	3	8.3	Kink	$-E_{SW}$
10	16-12-2014	15:46:44	[−1.26, 0.79, −0.84]	3	8.6	Steady	
11	17-12-2014	05:49:27	[−1.25, 0.28, 0.04]	3	7.9	Steady	
12	19-12-2014	21:43:32	[−1.21, 0.81, −0.70]	4	4.9	Steady	
13	28-12-2014	16:31:32	[−1.02, 0.937, −0.52]	3	4.4	Steady	
14	02-01-2015	01:54:43	[−0.93, 0.97, −0.41]	4	6.4	Steady	
15	02-01-2015	15:44:35	[−0.99, 0.80, −0.13]	3	3.5	Kink	$-E_{SW}$
16	01-03-2015	14:57:31	[−1.03, −0.15, 0.99]	7	3.1	Steady	
17	16-03-2015	20:16:35	[−1.15, 0.18, 1.05]	6	3.1	Kink	$-E_{SW}$
18	24-04-2015	13:09:34	[−1.780, 1.09 1.00]	5	3.1	Steady	
19	23-08-2015	03:49:55	[−1.10, −0.68, −0.20]	4	9.0	Steady	
20	24-08-2015	07:44:45	[−1.26, −0.79, 0.26]	5	3.0	Steady	
21	25-08-2015	02:15:36	[−1.28, −0.77, 0.25]	3	3.8	Kink	$-E_{SW}$
22	08-09-2015	07:12:10	[−1.23, −0.34, −0.42]	3	16.3	Kink	$-E_{SW}$
23	17-09-2015	10:04:56	[−1.31, −0.15, −0.49]	3	5.4	Steady	
24	18-09-2015	04:19:26	[−1.33, −0.14, −0.48]	3	6.5	Kink	$-E_{SW}$
25	21-09-2015	00:57:33	[−1.80, −0.09, 0.22]	3	3.2	Kink	$+E_{SW}$
26	23-09-2015	07:31:56	[−1.69, −0.02, −0.09]	3	4.4	Steady	
27	24-09-2015	01:33:35	[−1.29, −0.01, −0.60]	3	4.3	Kink	$+E_{SW}$
28	28-09-2015	05:48:52	[−1.48, 0.10, −0.47]	3	4.1	Steady	
29	29-09-2015	22:55:59	[−1.77, 0.19, −0.12]	3	3.2	Steady	
30	04-10-2015	02:59:54	[−1.73, 0.31, −0.25]	6	3.1	Steady	

After examining 504 orbits, we identified 106 events wherein multiple current sheet crossings were observed during a single tail traversal. Our statistical survey only includes events for which the MVA eigenvalue ratio (λ_2/λ_1) exceeded a value of three. This subset included a total of 70 events from which we definitively determined the flapping type for 30 events. The flapping types of the remaining 40 cases cannot be determined by using this technique. Of the 30 events that were successfully categorized, steady flapping was responsible for the multiple current sheet crossings in 20 events, while the remaining 10 were kink-like flapping events, generated by local wave propagations. Eight of these 10 kink-like flapping events have propagations traveling in the $-\mathbf{E_{SW}}$ direction. The results are summarized in Table 3, including the date, time, and location of the beginning of the interval when multiple current sheet crossings were observed. We also include information on the number of crossings for each event, *N*, the minimum eigenvalue ratio (λ_2/λ_1) in the set of crossings, whether the flapping is characterized as steady or kink-like flapping, and in the case of the latter, which direction the propagation was traveling ($+\mathbf{E_{SW}}$ or $-\mathbf{E_{SW}}$).

The spatial distribution of these flapping events is shown in MSE coordinates in Figure 8. The plotted location indicates MAVEN's position when the first crossing was observed in a multiple current sheet crossing series. The distribution of events does not indicate any preference for steady or kink-like flapping within different regions of the tail. We find that the kink-like flapping events propagating in the $-\mathbf{E_{SW}}$ direction are identified throughout the extent of the tail. This suggests that an energy source may exist at the outer flank of the tail, creating wave propagations in the opposite direction of the electric field. This observation is in contrast to observations in the magnetosphere of Venus and is discussed in further detail in section 5.

5. Discussion and Conclusions

We have reported statistical results on current sheet dynamics in the Martian magnetotail by using MAVEN MAG and SWIA data. Specifically, these dynamics have been investigated in the form of steady flapping,

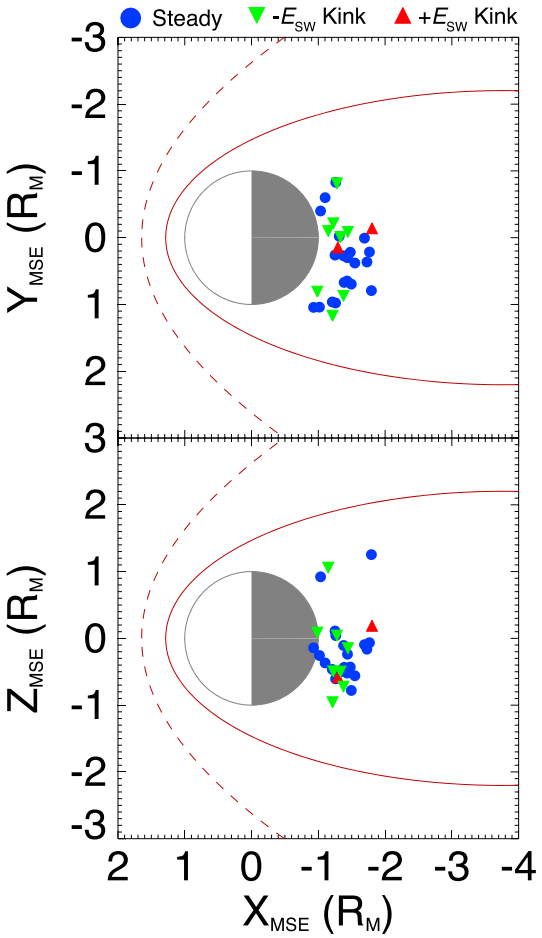


Figure 8. MAVEN's location at the start of each interval for the accepted steady and kink-like flapping events in the (a) equatorial (X_{MSE}-Y_{MSE}) plane and (b) meridional (X_{MSE}-Z_{MSE}) plane. Steady flapping events are denoted by a blue circle, kink-like flapping in the $+\mathbf{E_{SW}}$ direction are denoted by an upward red triangle, and kink-like flapping events in the $-\mathbf{E_{SW}}$ direction are marked by a downward green triangle. Nominal IMB and bow shock positions [*Trotignon et al.*, 2006] are indicated by red solid and dashed lines, respectively.

due to a global motion of the current sheet, and kink-like flapping, resulting from local wave propagations along the current sheet. The latter can provide evidence of possible energy sources in the magnetotail.

In the past it was difficult, if not impossible, to deduce between the steady and kink-like flapping using single-point measurements of multiple tail current sheet crossings. However, the technique developed by *Rong et al.* [2015a] provides a tool to distinguish between spatial and temporal changes in planetary magnetotail current sheets. We applied this method to MAVEN orbits occurring between 16 November 2014 and 31 October 2015 and identified 106 events where multiple current sheet crossings were observed over a single traversal of the tail. A total of 20 steady and 10 kink-like flapping events were identified.

The complexity of the Martian magnetotail was addressed in section 1, where we discussed how the textbook example of an induced magnetotail formed by the IMF draping around the planet might be complicated by the presence of crustal fields. In this work, we assumed that the magnetotail is formed by the draped IMF; however, because less than 50% of the multiple current sheet-crossing events were successfully categorized as steady or kink-like flapping, our paradigm of the dual-lobed Martian magnetotail may need further refinement to include crustal field affects on tail structure. Additional studies are needed to understand the configuration of the magnetic fields in the Martian magnetotail.

As we summarize the statistical results of this study, we compare our findings to those at the intrinsic magnetosphere of Earth [*Rong et al.*, 2015a] and the induced magnetosphere of Venus [*Rong et al.*, 2015b]. Current sheet flapping was identified at all three planets from steady, global motion and localized, kink-like waves. We find that unlike at Venus, steady flapping is much more common at Mars than the kink-like flapping type. After successfully classifying a total of 24 multiple current sheet-crossing events in the Venusian tail, *Rong et al.* [2015b] reported that nine were identified as steady flapping and 15 as kink-like flapping.

Kink-like flapping events at both Mars and Venus were found throughout the entire magnetotail. This differs from Earth where kink-like propagations are confined to the central tail and propagate toward the flanks in the dawnward and duskward directions [e.g., *Zhang et al.*, 2002; *Sergeev et al.*, 2003, 2004]. Although we still do not know the exact mechanisms and energy sources driving these kink-like waves, current theories include magnetohydrodynamic waves [e.g., *Golovchanskaya and Maltsev*, 2005; *Erkaev et al.*, 2007, 2009], Kelvin-Helmholtz instabilities [e.g., *Nakagawa and Nishida*, 1989], magnetic reconnection [e.g., *Øieroset*

et al., 2001; *Sergeev et al*., 2006], and IMF Alfvénic wave penetration [*Toyichi and Miyazak*, 1976]. At Mars, Alfvénic waves are the dominant wave mode observed throughout the magnetosheath and magnetosphere [*Ruhunusiri et al*., 2015], suggesting that Alfvénic wave penetration is a viable mechanism for creating these kink-like propagations.

A majority of the kink-like events at Mars were generated from wave propagation in the $-\mathbf{E_{SW}}$ direction along the current sheet. That is, eight out of the 10 kink-like events were from waves propagating in the opposite direction of the solar wind convection electric field, while only two of the kink-like events were generated from waves propagating in the $+\mathbf{E_{SW}}$ direction. This pattern was not observed at Venus, where *Rong et al*. [2015b] reported an equal distribution between $-\mathbf{E_{SW}}$- and $+\mathbf{E_{SW}}$-traveling kink-like propagations. They suggested that Venus might have an energy source at the flanks of tail, creating propagations toward the center [see *Rong et al*., 2015b, Figure 5c].

We conclude that the Mars energy source is most likely not located near the central tail because our results indicate a preference for wave propagation in the $-\mathbf{E_{SW}}$ direction throughout the magnetotail. At Venus, statistical surveys [e.g., *Zhang et al*., 2010; *Rong et al*., 2014] demonstrated that magnetic reconnection might occur more frequently near the $-\mathbf{E_{SW}}$ flank of the tail. Although no similar statistical investigation has been performed at Mars, case studies of magnetic reconnection have been reported in the Martian magnetotail [e.g., *Eastwood et al*., 2008; *DiBraccio et al*., 2015; *Harada et al*., 2015a]. If there is a preference for magnetic reconnection in the $+\mathbf{E_{SW}}$ tail flank at Mars, it could be responsible for the $-\mathbf{E_{SW}}$-traveling kink-like events; however, a more extensive study is needed to determine this.

Previous studies at Mars have addressed various topics that could generate this kink-like flapping. *DiBraccio et al*. [2015] reported signatures of tail loading and unloading, which is the repetitive and dramatic increase-then-decrease of magnetic flux as the field magnitude changes by up to a factor of six over short intervals of several minutes. This loading and unloading of tail flux is caused by magnetic reconnection, exhibits signatures similar to substorm activity within intrinsic magnetospheres, and may create impulsive energy sources, triggering kink-like waves as the tail reconnects. *Dubinin et al*. [2012] reported observations of bursty plasma flows, possibly associated with reconnection in the Martian magnetotail; however, the lack of simultaneous plasma and magnetic field measurements onboard Mars Express (MEX) made it impossible to assess whether these flows were associated with current sheet flapping. In addition to magnetic reconnection, Kelvin-Helmhotz instabilities have recently been identified at Mars [*Ruhunusiri et al*., 2016]. These boundary oscillations could potentially trigger waves along the current sheet from the outer flank and through the magnetotail.

The $-\mathbf{E_{SW}}$ preference of the kink-like flapping events may also explain previous observations of plasma dynamics in the Martian tail. Using MEX data, *Winningham et al*. [2006] reported intervals of electron bursts in the Martian magnetotail, observed as periodic electron oscillations, which may be a direct effect of tail flapping. In a study of tailward transport of suprathermal (>25 eV) planetary ions using MAVEN data, *Harada et al*. [2015b] reported enhancements of the net Marsward flux of protons and tailward flux of oxygen ions in the $-\mathbf{E_{SW}}$ hemisphere. *Harada et al*. [2015b] also observed an average weaker magnetic field intensity, with an enhanced B_Y component in the $-\mathbf{E_{SW}}$ hemisphere of the tail when compared to the $+\mathbf{E_{SW}}$ hemisphere.

As MAVEN continues to collect data in the Martian magnetotail, increased statistics of tail dynamics are necessary to fully understand the energy sources that affect the current sheet. Future studies will include analysis of plasma data during these current sheet crossings in order to understand how particles are affected by steady and kink-like flapping. In this work we have concluded that of the selected events, a majority of the multiple current sheet crossings were due to steady flapping rather than kink-like waves propagating along the current sheet. These kink-like events, however, are observed to travel mostly in the opposite direction to the solar wind electric field. As we enhance our understanding of the structure and dynamics of Mars' magnetotail, we are able to identify the mechanisms responsible for the loss of atmospheric particles to space.

Acknowledgments
The MAVEN project is supported by NASA through the Mars Exploration Program. MAVEN data are publicly available through the Planetary Data System. This research was supported by a NASA Postdoctoral Program appointment at the NASA Goddard Space Flight Center, administered by Universities Space Research Association (USRA) through a contract with NASA.

References

Acuña, M. H., et al. (1998), Magnetic field and plasma observations at Mars: Initial results of the Mars global surveyor mission, *Science*, *279*, 1676–1680, doi:10.1126/Science.279.5357.1676.

Barabash, S., A. Fedorov, R. Lundin, and J. A. Sauvaud (2007), Martian atmospheric erosion rates, *Science*, *315*, 501, doi:10.1126/science.1134358.

Brain, D. A., et al. (2015), The spatial distribution of planetary ion fluxes near Mars observed by MAVEN, *Geophys. Res. Lett.*, *42*, 9142–9148, doi:10.1002/2015GL065293.
Connerney, J. E. P., M. H. Acuña, N. F. Ness, G. Kletetschka, D. L. Mitchell, R. P. Lin, and H. Reme (2005), Tectonic implications of Mars crustal magnetism, *Proc. Natl. Acad. Sci. U.S.A.*, *102*, 14,970–14,975, doi:10.1073/Pnas.0507469102.
Connerney, J. E. P., J. Espley, P. Lawton, S. Murphy, J. Odom, R. Oliversen, and D. Sheppard (2015), The MAVEN magnetic field investigation, *Space Sci. Rev.*, doi:10.1007/s11214-015-0169-4.
Crider, D. H., D. A. Brain, M. H. Acuña, D. Vignes, C. Mazelle, and C. Bertucci (2004), Mars Global Surveyor observations of solar wind magnetic field draping around Mars, *Space Sci. Rev.*, *111*, doi:10.1023/B:SPAC.0000032714.66124.4e.
DiBraccio, G. A., et al. (2015), Magnetotail dynamics at Mars: Initial MAVEN observations, *Geophys. Res. Lett.*, *42*, 8828–8837, doi:10.1002/2015GL065248.
Dong, Y., X. Fang, D. A. Brain, J. P. McFadden, J. S. Halekas, J. E. Connerney, S. M. Curry, Y. Harada, J. G. Luhmann, and B. M. Jakosky (2015), Strong plume fluxes at Mars observed by MAVEN: An important planetary ion escape channel, *Geophys. Res. Lett.*, *42*, 8942–8950, doi:10.1002/2015GL065346.
Dubinin, E., R. Lundin, W. Riedler, K. Schwingenschuh, J. G. Luhmann, C. T. Russell, and L. H. Brace (1991), Comparison of observed plasma and magnetic-field structures in the wakes of Mars and Venus, *J. Geophys. Res.*, *96*, 11,189–11,197, doi:10.1029/91JA01102.
Dubinin, E., R. Lundin, H. Koskinen, and N. Pissarenko (1993), Ion acceleration in the Martian tail: Phobos observations, *J. Geophys. Res.*, *98*, 3991–3997, doi:10.1029/92JA02233.
Dubinin, E., M. Fraenz, A. Fedorov, R. Lundin, N. Edberg, F. Duru, and O. Vaisberg (2011), Ion energization and escape on Mars and Venus, *Space Sci. Rev.*, *162*, doi:10.1007/s11214-011-9831-7.
Dubinin, E., M. Fraenz, J. Woch, T. L. Zhang, J. Wei, A. Fedorov, S. Barabash, and R. Lundin (2012), Bursty escape fluxes in plasma sheets of Mars and Venus, *Geophys. Res. Lett.*, *39*, L01104, doi:10.1029/2011GL049883.
Eastwood, J. P., D. A. Brain, J. S. Halekas, J. F. Drake, T. D. Phan, M. Øieroset, D. L. Mitchell, R. P. Lin, and M. Acuña (2008), Evidence for collisionless magnetic reconnection at Mars, *Geophys. Res. Lett.*, *35*, L02106, doi:10.1029/2007GL032289.
Erkaev, N. V., V. S. Semenov, and H. K. Biernat (2007), Magnetic double gradient instability and flapping waves in a current sheet, *Phys. Rev. Lett.*, *99*, doi:10.1103/PhysRevLett.99.235003.
Erkaev, N. V., V. S. Semenov, I. V. Kubyshkin, M. V. Kubyshkina, and H. K. Biernat (2009), MHD model of the flapping motions in the magnetotail current sheet, *J. Geophys. Res.*, *114*, A03206, doi:10.1029/2008JA013728.
Escoubet, C. P., M. Fehringer, and M. Goldstein (2001), The Cluster mission, *Ann. Geophys.*, *19*, doi:10.5194/angeo-19-1197-2001.
Fedorov, A., et al. (2006), Structure of the Martian wake, *Icarus*, *182*, doi:10.1016/j.icarus.2005.09.021.
Golovchanskaya, I. V., and Y. P. Maltsev (2005), On the identification of plasma sheet flapping waves observed by Cluster, *Geophys. Res. Lett.*, *32*, L02102, doi:10.1029/2004GL021552.
Halekas, J. S., D. A. Brain, R. J. Lillis, M. O. Fillingim, D. L. Mitchell, and R. P. Lin (2006), Current sheets at low altitudes in the Martian magnetotail, *Geophys. Res. Lett.*, *33*, L13101, doi:10.1029/2006GL026229.
Halekas, J. S., J. P. Eastwood, D. A. Brain, T. D. Phan, M. Oieroset, and R. P. Lin (2009), In situ observations of reconnection Hall magnetic fields at Mars: Evidence for ion diffusion region encounters, *J. Geophys. Res.*, *114*, A11204, doi:10.1029/2009JA014544.
Halekas, J. S., E. R. Taylor, G. Dalton, G. Johnson, D. W. Curtis, J. P. McFadden, D. L. Mitchell, R. P. Lin, and B. M. Jakosky (2015), The solar wind ion analyzer for MAVEN, *Space Sci. Rev.*, doi:10.1007/s11214-013-0029-z.
Halekas, J. S., et al. (2016), Plasma clouds and snowplows: Bulk plasma escape from Mars observed by MAVEN, *Geophys. Res. Lett.*, *43*, 1426–1434, doi:10.1002/2016GL067752.
Halekas, J. S., et al. (2017), Structure, dynamics, and seasonal variability of the Mars-solar wind interaction: MAVEN Solar Wind Ion Analyzer in-flight performance and science results, *Geophys. Res. Space Physics*, *122*, 547–578, doi:10.1002/2016JA023167.
Hara, T., et al. (2015), Estimation of the spatial structure of a detached magnetic flux rope at Mars based on simultaneous MAVEN plasma and magnetic field observations, *Geophys. Res. Lett.*, *42*, 8933–8941, doi:10.1002/2015GL065720.
Hara, T., et al. (2016), MAVEN observations of magnetic flux ropes with a strong field amplitude in the Martian magnetosheath during the ICME passage on 8 March 2015, *Geophys. Res. Lett.*, *43*, 4816–4824, doi:10.1002/2016GL068960.
Harada, Y., et al. (2015a), Magnetic reconnection in the near-Mars magnetotail: MAVEN observations, *Geophys. Res. Lett.*, *42*, 8838–8845, doi:10.1002/2015GL065004.
Harada, Y., et al. (2015b), Marsward and tailward ions in the near-Mars magnetotail: MAVEN observations, *Geophys. Res. Lett.*, *42*, 8925–8932, doi:10.1002/2015GL065005.
Jakosky, B. M., et al. (2015), The Mars Atmosphere and Volatile Evolution (MAVEN) mission, *Space Sci. Rev.*, *195*, doi:10.1007/s11214-015-0139-x.
Luhmann, J. G., C. T. Russell, K. Schwingenschuh, and Y. Yeroshenko (1991), A comparison of induced magnetotails of planetary bodies: Venus, Mars and Titan, *J. Geophys. Res.*, *96*, 11,199–11,208, doi:10.1029/91JA00086.
Luhmann, J. G., et al. (2015), Implications of MAVEN Mars near-wake measurements and models, *Geophys. Res. Lett.*, *42*, 9087–9094, doi:10.1002/2015GL066122.
Lundin, R., and S. Barabash (2004), The wakes and magnetotails of Mars and Venus, *Adv. Space Res.*, *33*, doi:10.1016/j.asr.2003.07.054.
Morschhauser, A., V. Lesur, and M. Grott (2014), A spherical harmonic model of the lithospheric magnetic field of Mars, *J. Geophys. Res. Planets*, *119*, 1162–1188, doi:10.1002/2013JE004555.
Nakagawa, T., and A. Nishida (1989), Southward magnetic field in the neutral sheet produced by wavy motions in the dawn-dusk direction, *Geophys. Res. Lett.*, *11*, 1265–1268, doi:10.1029/GL016i011p01265.
Øieroset, M., T. D. Phan, M. Fujimoto, R. P. Lin, and R. P. Lepping (2001), In situ detection of collisionless reconnection in the Earth's magnetotail, *Nature*, *412*, 414–417, doi:10.1038/35086520.
Romanelli, N., C. Bertucci, D. Gómez, and C. Mazelle (2015), Dependence of the location of the Martian magnetic lobes on the interplanetary magnetic field direction: Observations from Mars Global Surveyor, *J. Geophys. Res. Space Physics*, *120*, 7737–7747, doi:10.1002/2015JA021359.
Rong, Z. J., S. Barabash, Y. Futaana, G. Stenberg, T. L. Zhang, W. X. Wan, Y. Wei, X.-D. Wang, L. H. Chai, and J. Zhong (2014), Morphology of magnetic field in near-Venus magnetotail: Venus express observations, *J. Geophys. Res. Space Physics*, *119*, 8838–8847, doi:10.1002/2014JA020461.
Rong, Z. J., S. Barabash, G. Stenberg, Y. Futaana, T. L. Zhang, W. X. Wan, Y. Wei, and X.-D. Wang (2015a), Technique for diagnosing the flapping motion of magnetotail current sheets based on single-point magnetic field analysis, *J. Geophys. Res. Space Physics*, *120*, 3462–3474, doi:10.1002/2014JA020973.

Rong, Z. J., S. Barabash, G. Stenberg, Y. Futaana, T. L. Zhang, W. X. Wan, Y. Wei, X. D. Wang, L. H. Chai, and J. Zhong (2015b), The flapping motion of the Venusian magnetotail: Venus Express observations, *J. Geophys. Res. Space Physics*, *120*, 5593–5602, doi:10.1002/2015JA021317.

Ruhunusiri, S., J. S. Halekas, J. E. P. Connerney, J. R. Espley, J. P. McFadden, D. E. Larson, D. L. Mitchell, C. Mazelle, and B. M. Jakosky (2015), Low-frequency waves in the Martian magnetosphere and their response to upstream solar wind driving conditions, *Geophys. Res. Lett.*, *42*, 8917–8924, doi:10.1002/2015GL064968.

Ruhunusiri, S., et al. (2016), MAVEN observations of partially developed Kelvin-Helmholtz vortices at Mars, *Geophys. Res. Lett.*, *43*, 4763–4773, doi:10.1002/2016GL068926.

Sergeev, V., et al. (2003), Current sheet flapping motion and structure observed by Cluster, *Geophys. Res. Lett.*, *30*(13), 1712, doi:10.1029/2002GL016500.

Sergeev, V., A. Runov, W. Baumjohann, R. Nakamura, T. L. Zhang, A. Balogh, P. Louarn, J.-A. Sauvaud, and H. Reme (2004), Orientation and propagation of current sheet oscillations, *Geophys. Res. Lett.*, *31*, L05807, doi:10.1029/2003GL019346.

Sergeev, V. A., D. A. Sormakov, S. V. Apatenkov, W. Baumjohann, R. Nakamura, A. V. Runov, T. Mukai, and T. Nagai (2006), Survey of large amplitude flapping motions in the midtail current sheet, *Ann. Geophys.*, *24*, doi:10.5194/angeo-24-2015-2006.

Sonnerup, B. U. Ö., and L. J. Cahill Jr. (1967), Magnetopause structure and attitude from Explorer 12 observations, *J. Geophys. Res.*, *72*, 171–183, doi:10.1029/JZ072i001p00171.

Sonnerup, B. U. Ö., and M. Scheible (1998), Minimum and maximum variance analysis, in *Analysis Methods for Multi-Spacecraft Data*, *ISSI Sci. Rep. no. SR-001*, edited by G. Paschmann and P. W. Daly, chap. 8, pp. 185–220, European Space Agency, Noordwijk, Netherlands.

Toyichi, T., and T. Miyazak (1976), Flapping motions of the tail plasma sheet induced by the interplanetary magnetic field variations, *Planet. Space Sci.*, *24*, doi:10.1016/0032-0633(76)90102-1.

Trotignon, J. G., C. Mazelle, C. Bertucci, and M. H. Acuña (2006), Martian shock and magnetic pile-up boundary positions and shapes determined from the Phobos 2 and Mars Global Surveyor data sets, *Planet. Space Sci.*, *54*, 357–369, doi:10.1016/J.Pss.2006.01.003.

Vaisberg, O. L. (1992), The solar wind interaction with Mars: A review of results from early Soviet missions to Mars, in *Venus and Mars: Atmospheres, Ionospheres and Solar Wind Interactions*, vol. 66, pp. 311–326, AGU Monogr., Washington, D. C.

Winningham, J. D., et al. (2006), Electron oscillations in the induced Martian magnetosphere, *Icarus*, *182*, doi:10.1016/j.icarus.2005.10.033.

Yeroshenko, Y., W. Riedler, K. Schwingenschuh, J. G. Luhmann, M. Ong, and C. T. Russell (1990), The magnetotail of Mars: Phobos observation, *Geophys. Res. Lett.*, *17*, 885–888, doi:10.1029/GL017i006p00885.

Zhang, T. L., W. Baumjohann, R. Nakamura, A. Balogh, K.-H. Glassmeier (2002), A wavy twisted neutral sheet observed by Cluster, *Geophys. Res. Lett.*, *29*(19), 1899, doi:10.1029/2002GL015544.

Zhang, T. L., W. Baumjohann, J. Du, R. Nakamura, R. Jarvinen, E. Kallio, A. M. Du, M. Balikhin, J. G. Luhmann, and C. T. Russell (2010), Hemispheric asymmetry of the magnetic field wrapping pattern in the Venusian magnetotail, *Geophys. Res. Lett.*, *37*, L14202, doi:10.1029/2010GL044020.

Zhang, T.-L., K. Schwingenschuh, C. T. Russell, J. G. Luhmann, H. Rosenbauer, M. I. Verigin, and G. Kotova (1994), The flaring of the Martian magnetotail observed by the Phobos 2 spacecraft, *Geophys. Res. Lett.*, *21*, 1121–1124, doi:10.1029/94GL01073.